Nuclear Magnetic Resonance Investigations of a Novel Intramolecular Methylthio Replacement Process in Palladium(II) and Platinum(II) Complexes of Mixed Sulfur–Phosphine Ligands *

Edward W. Abel,[a] Jonathan C. Dormer,[a] David Ellis,[a] Keith G. Orrell,[a] Vladimir Šik,[a] Michael B. Hursthouse[b] and Mohammed A. Mazid[b]

[a] *Department of Chemistry, The University, Exeter EX4 4QD, UK*

[b] *Department of Chemistry, Queen Mary and Westfield College, London E1 4NS, UK*

A series of palladium(II) and platinum(II) complexes with the mono- and bis-chelate ligands bis[*o*-(methylthio)phenyl]phenylphosphine and tris[*o*-(methylthio)phenyl]phosphine have been prepared and characterised. Despite the potential tridenticity of the first ligand it acts as a P/S monochelate to form square-planar complexes of type $[M\{PPh(C_6H_4SMe\text{-}o)_2\}X_2]$ (M = Pd, X = Cl, Br or I; M = Pt, X = Cl). Variable-temperature one- and two-dimensional NMR spectroscopy showed that pyramidal inversion of the co-ordinated sulfur atoms was accompanied by an exchange of pendant and bound methylthio groups. The $\Delta G^{\ddagger}$ values for both processes were in the range 43–69 kJ mol^{-1}, being strongly metal and halogen dependent. The bis(chelate) complexes $[M\{P(C_6H_4SMe\text{-}o)_3\}_2][ClO_4]_2$ are also square planar with metal co-ordination involving one phosphorus and one sulfur of each ligand, the other two pairs of SMe groups being unco-ordinated. The X-ray crystal structure of $[Pd\{P(C_6H_4SMe\text{-}o)_3\}_2][ClO_4]_2$ shows the co-ordinated *S*-methyls to be mutually *cis* with respect to the metallocycle plane. In low-temperature solutions of this complex this *cis* form is assumed to be predominant. At higher solution temperatures a facile intramolecular exchange of all six methylthio groups occurs. The energy and probable mechanism of this fluxion are reported.

In connection with a general investigation of the static and dynamic structures of transition-metal complexes with hybrid sulfur–phosphine ligands we have recently examined complexes of bis[*o*-(methylthio)phenyl]phenylphosphine with rhenium(I) pentacarbonyl halides.[1] This ligand acts as a S/P monochelate, and the complexes contain one bound and one unbound *S*-methyl group at all temperatures. However, in 1974 Lockyer[2] examined the ^{1}H NMR spectrum of the palladium(II) complex $[Pd\{PPh(C_6H_4SMe\text{-}o)_2\}_2Cl_2]$ and noted a broad singlet *S*-methyl signal. Since previous results from electronic spectroscopy[3] had suggested a square-planar complex with the ligand bonding through phosphorus and a single sulfur atom, he suggested that an intramolecular exchange of free and bound SMe groups might be occurring.

We have now pursued this suggestion in order to establish whether such a process does indeed occur in palladium(II) and platinum(II) complexes of this ligand in contrast to rhenium(I) complexes where it was found to be absent,[1] and, if so, how its rates compare with that of pyramidal inversion of the bound SMe groups.[4,5] The complexes investigated are $[M\{PPh(C_6H_4SMe\text{-}o)_2\}X_2]$ (M = Pd, X = Cl, Br or I; M = Pt, X = Cl). We have also extended the study to include the complexes of the bis(chelate ligand) tris[*o*-(methylthio)phenyl]phosphine, namely $[M\{P(C_6H_4SMe\text{-}o)_3\}_2][ClO_4]_2$ (M = Pd or Pt), in order to establish whether an analogous SMe replacement fluxion occurs in these species.

Experimental

Materials.—All preparations were carried out using standard Schlenk procedures. Elemental analyses were performed by Butterworth Laboratories, Teddington, Middlesex. Melting points were recorded on a digital Gallenkamp apparatus and were uncorrected.

The ligands[6] and the metal precursor, $[PtCl_2(PhCN)_2]$,[7] were prepared in good yield from standard literature methods. Preparative details of the complexes are as follows.

$[Pd\{PPh(C_6H_4SMe\text{-}o)_2\}X_2]$ (X = Cl **1**, Br **2** or I **3**). The dichloro- and diiodo-complexes have been synthesised previously.[3,8] The method of Livingstone and Lockyer[8] was adopted for this study. A solution of potassium tetrachloropalladate(II) (0.32 g, 1.0 mmol) in distilled water (5 cm^3) was added to a solution of $PPh(C_6H_4SMe\text{-}o)_2$ (0.35 g, 1.0 mmol) in warm acetone. A yellow-orange solid was filtered off, washed with hexane and recrystallised from dichloromethane–hexane (1:1). Yield 0.40 g. Formation of the other halide complexes was accomplished similarly, but with the addition of an excess of lithium bromide or iodide to the boiling acetone solution before mixing with potassium tetrachloropalladate.

$[Pt\{PPh(C_6H_4SMe\text{-}o)_2\}Cl_2]$ **4**. The ligand $PPh(C_6H_4SMe\text{-}o)_2$ (0.11 g, 0.3 mmol) and $[PtCl_2(PhCN)_2]$ (0.158 g, 0.33 mmol) were added to cold benzene (10 cm^3). The ligand dissolved readily whereas $[PtCl_2(PhCN)_2]$ dissolved only when the mixture was heated under reflux at 70 °C. After 10 min an orange solid precipitated out of the yellow solution. After filtering and drying *in vacuo* orange crystals were obtained. Yield 0.12 g.

$[Pd\{P(C_6H_4SMe\text{-}o)_3\}_2][ClO_4]_2$ **5**. This complex has been prepared previously by Meek and co-workers.[3] A solution of sodium tetrachloropalladate(II) (0.27 g, 0.78 mmol) in ethanol (10 cm^3) was added to a suspension of $P(C_6H_4SMe\text{-}o)_3$ (0.64 g, 1.55 mmol) in hot ethanol, containing lithium perchlorate (0.38 g, 3.57 mmol). The mixture was stirred at room temperature for 45 min after which time a deep red precipitate was filtered off, dried *in vacuo* and recrystallised from dichloromethane–butan-1-ol (1:1). Yield 0.38 g.

* *Supplementary data available:* see Instructions for Authors, *J. Chem. Soc., Dalton Trans.*, 1992, Issue 1, pp. xx–xxv.

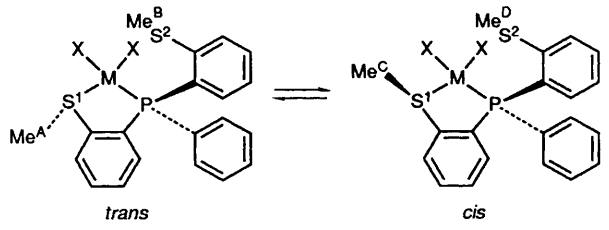

Fig. 1 Isomeric structures of the $[M\{PPh(C_6H_4SMe\text{-}o)_2\}X_2]$ complexes, showing the labelling of the SMe environments

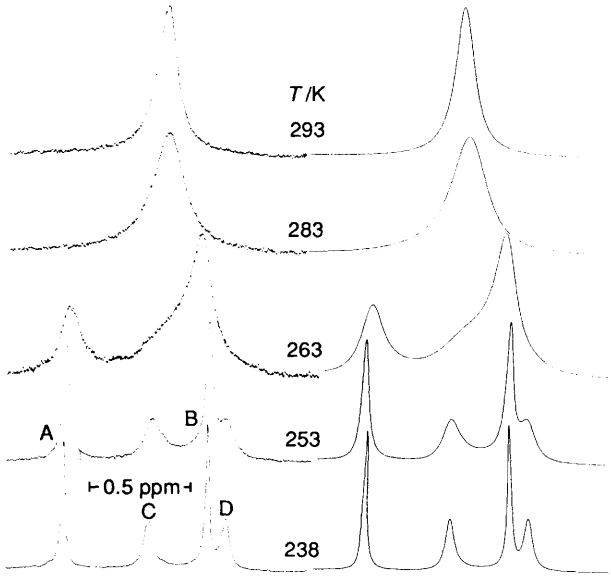

Fig. 2 Experimental and computer-simulated ^1H NMR spectra of $[Pd\{PPh(C_6H_4SMe\text{-}o)_2\}Cl_2]$

$[Pt\{P(C_6H_4SMe\text{-}o)_3\}_2][ClO_4]_2$ **6**. This complex has not been reported previously. The complex $[PtCl_2(PhCN)_2]$ (0.12 g, 0.25 mmol) and the ligand $P(C_6H_4SMe\text{-}o)_3$ (0.20 g, 0.50 mmol) were added to warm methanol (20 cm^3). The mixture was heated and stirred to dissolution, and stirring continued for 30 min. Sodium perchlorate (0.18 g, 1.25 mmol) was added and the solution concentrated *in vacuo* to yield a yellow solid. This was recrystallised from dichloromethane–hexane (1:1) to give yellow crystals. Yield 0.17 g.

Characterisation data for the complexes **1**–**6** are given in Table 1.

NMR Spectra.—Proton NMR spectra were recorded on a Bruker AM 250 FT spectrometer operating at 250.13 MHz. Shifts are quoted relative to $SiMe_4$ as internal standard. A BVT-1000 unit was used to control the magnet probe temperature, the calibration of this unit being checked regularly against a Comark digital thermometer. Quoted temperatures are accurate to ± 1 °C. Two-dimensional ^1H exchange spectroscopy (EXSY) spectra were recorded on complexes **1** and **3** using the Bruker automation program NOESYPH, with the pulse sequence D1–90°–D0–90°–D9–90°–free induction decay (FID). The relaxation delay D1 was set at 2 s, and the evolution time D0 had an initial value of 3×10^{-6} s. The mixing time D9 varied between 0.07 and 0.5 s according to the complex and measurement temperature. The frequency domain F1 contained 512 words, zero filled to 1000 words, and F2 contained 1000 words. The spectral width was typically set at 250–300 Hz and the number of pulses at 16. Data processing incorporated an exponential window function with a line broadening of 0.5 Hz. Rate data were extracted from the two-dimensional EXSY contour plots using the D2DNMR program described previously.[9–11]

Rate data from one-dimensional spectra were based on total bandshape analysis using the author's version of the DNMR3 program,[12] and involving visual fittings of experimental and calculated spectra. Activation parameters based on one- and two-dimensional derived rate data were calculated using the THERMO program.[13]

X-Ray Crystal Structure.—Crystals of $[Pd\{P(C_6H_4SMe\text{-}o)_3\}_2][ClO_4]_2$ **5** were prepared as described above and sealed under nitrogen in Lindemann capillaries.

Crystal data. $[C_{42}H_{42}P_2PdS_6][ClO_4]_2$, $M = 1106.46$, monoclinic, space group $P2_1/a$, $a = 22.632(7)$, $b = 14.232(3)$, $c = 14.511(3)$ Å, $\beta = 94.83(2)°$, $U = 4657.38$ Å^3, $Z = 4$, $D_c = 1.58$ g cm^{-3}, $F(000) = 2256$. Radiation Mo-Kα, $\lambda = 0.710\,69$ Å, $\mu = 8.835$ cm^{-1}.

Data collection. CAD4 Diffractometer with graphite-monochromatised Mo-Kα radiation, 6973 reflections measured ($1.5 \leqslant \theta \leqslant 23.0°$) giving 6467 unique and 3838 observed with $F_o > 3\sigma(F_o)$.

Structure analysis and refinement. The structure was solved by normal heavy-atom procedures (SHELX 84).[14] Full-matrix least-squares refinement (SHELX 76)[15] was performed with all non-hydrogen atoms assigned anisotropic thermal parameters. Hydrogen atoms were experimentally located and freely refined with group U_{iso} values. The number of parameters in the least-squares scheme was 625. The weighting scheme $w = 1/[\sigma^2(F_o) + g(F_o)^2]$ with $g = 0.001\,542$ gave satisfactory agreement analyses. Final R and R_G values were 0.059 and 0.068 respectively. Perchlorate anion Cl(2) is extensively disordered.

Additional material available from the Cambridge Crystallographic Data Centre comprises H-atom coordinates, thermal parameters and remaining bond lengths and angles.

Results and Discussion

(*i*) $[Pd\{PPh(C_6H_4SMe\text{-}o)_2\}X_2]$ *Complexes.*—The structures of these previously established square-planar complexes[3] are given in Fig. 1. Co-ordination occurs through the phosphorus atom and *one* of the methylthio groups producing metal(II) *cis*-chelate complexes. Low-temperature ^1H NMR spectra provide full characterisation of these structures. Each complex in solution gives rise to *two* pairs of *S*-methyl signals (Fig. 2) and complex aromatic absorption. The number of *S*-methyl signals indicates the presence of non-exchanging pairs of *cis* and *trans* isomers (invertomers) of the complexes. The higher-frequency pair of signals is attributed to the co-ordinated SMe groups and the lower-frequency pair to the unco-ordinated pendant SMe groups. The relative intensities of the signals provide estimates of the solution populations of the invertomers. These vary according to the nature of the halogen (Table 2). In the $[Pd\{PPh(C_6H_4SMe\text{-}o)_2\}_2X_2]$ complexes, when X is varied from Cl to Br to I, there is a regular decrease in the population of the *trans* species and concomitant gain in population of the *cis* species such that when X = I this species is more populous. This trend is analogous to those found for the complexes *cis*-$[PdX_2L]$ [L = MeSCH=CHMe or *o*-$(SMe)_2C_6H_3Me$].[16]

The four SMe signals in the low-temperature ^1H NMR spectra of each of the $PPh(C_6H_4SMe\text{-}o)_2$ complexes are assigned unambiguously, with the highest-frequency pair being due to the co-ordinated SMe groups A and C (Fig. 1). On raising the solution temperature of the complexes the spectra become temperature dependent. Signals due to SMe groups B and D coalesce initially to give an averaged signal which coalesces with C and then finally with A to give a single broad line which sharpens on further elevation of sample temperature. Addition of free ligand at this stage reveals no exchange between signals due to free and complexed ligand.

In order to explain these signal averagings, two rate processes must be invoked, namely pyramidal inversion of the co-ordinated S atom and internal *S*-methyl replacement causing exchange between co-ordinated and unco-ordinated *S*-methyl groups. Full consideration of the kinetics requires the scheme

Table 1 Characterisation data for the complexes

Complex	Yield (%)	Colour	M.p./°C	Analytical data (%) Calc. C	Calc. H	Found C	Found H
1 $[Pd\{PPh(C_6H_4SMe\text{-}o)_2\}Cl_2]$	82	Orange	200	44.30	3.45	45.20	3.60
2 $[Pd\{PPh(C_6H_4SMe\text{-}o)_2\}Br_2]$	70	Orange	198	38.20	3.10	38.70	3.05
3 $[Pd\{PPh(C_6H_4SMe\text{-}o)_2\}I_2]$	70	Red	195	33.90	2.75	33.60	2.80
4 $[Pt\{PPh(C_6H_4SMe\text{-}o)_2\}Cl_2]$	57	Yellow	*		*		*
5 $[Pd\{P(C_6H_4SMe\text{-}o)_3\}_2][ClO_4]_2$	41	Red	243	45.30	3.75	46.60	3.80
6 $[Pt\{P(C_6H_4SMe\text{-}o)_3\}_2][ClO_4]_2$	56	Yellow	270	41.20	3.50	42.20	3.55

* No data available.

Table 2 Proton NMR parameters of complexes **1**–**6** at low temperature

Complex	M	T/°C	Invertomer population	Chemical shifts δ SMe protons	Aromatic protons
1	Pd	−40	0.57	3.15,[a] 2.47	7.1–8.1
			0.43	2.76,[a] 2.37	
2	Pd	−70	0.49	3.22,[a] 2.45	7.0–8.1
			0.51	2.79,[a] 2.39	
3	Pd	−80	0.34	3.23,[a] 2.38	7.0–8.0
			0.66	2.76,[a] 2.28	
4	Pt	10	0.52	3.23[a] (50.0),[b] 2.40	7.0–8.0
			0.48	2.81[a] (43.7),[b] 2.34	
5	Pd	−90	0.96[c]	2.46,[d] 2.19,[d] 2.06[d]	6.9–8.0
			0.04[c]		
6	Pt	−70		2.51, 2.35 (43.3),[b] 2.07	7.0–7.9

[a] Chemical shift of co-ordinated SMe in complexes **1**–**4** given first. [b] ^3J(Pt–H)/Hz. [c] Based on $^{31}P\text{-}\{^1H\}$ NMR spectrum at −85 °C. [d] Value for *cis* invertomer.

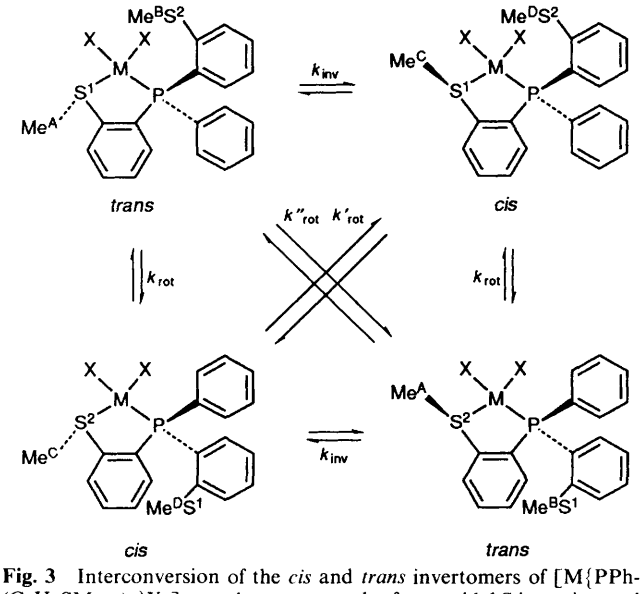

Fig. 3 Interconversion of the *cis* and *trans* invertomers of $[M\{PPh(C_6H_4SMe\text{-}o)_2\}X_2]$ complexes as a result of pyramidal S inversion and SMe replacement

shown in Fig. 3. Both *cis* and *trans* invertomers exist as DL pairs which differ simply in the labelling of the SMe groups. Exchange between these DL pairs is therefore NMR detectable, and exchange involving the whole set of four invertomers requires a total of six rate constants. However, symmetry reduces this number to four, namely the inversion rate constant, k_{inv}, and three *S*-methyl replacement rate constants. These all involve initial easing of the M–S bonding followed by a rotation about the M–P bond through the tetrahedral angle to bring the pendant *S*-methyl close enough for participation in a five-co-ordinate metal transition state and thence to displace the previously bound *S*-methyl. These rotation rate constants are defined as k_{rot} when the exchange involves *cis*–*trans* invertomer exchange, k'_{rot} when the process involves a labelling exchange of the *cis* invertomers, and k''_{rot} when the process has an analogous effect on the *trans* pair. It was clear from an initial examination of the ^1H NMR spectra that some of the rate constants were of comparable magnitude and that bandshape fitting to four independent rate constants would be impracticable. Resort was therefore made to two-dimensional EXSY experiments which are known to be particularly powerful for slow, multi-site exchange problems.[9–11] The method is only valid for spectra in the slow-exchange regime which show no effects of dynamic broadening. For complexes **1** and **3** this required spectra to be measured in the temperature ranges −40 to −60 and −80 to −90 °C, respectively. A typical ^1H two-dimensional EXSY spectrum of the SMe region is shown in Fig. 4. The off-diagonal signals are generated by magnetisation transfer resulting from the chemical exchange process. The intensities of the signals relative to the diagonal signal intensities enable the magnitudes of four rate constants to be independently measured. The dynamic spin problem for the system is of the type shown in Scheme 1. However, this can be simplified to that in Scheme 2 since there is no observable scalar coupling or cross-relaxation between the pairs of *S*-methyl protons in each species.

The results obtained for complexes **1** and **3** using our D2DNMR program[9] are given in Table 3. It is clear that over this limited low-temperature range the kinetics is dominated by the SMe replacement rate constants k_{rot} and k'_{rot}, the other rates being negligibly slow at these low temperatures. In order to check the reliability of these values, magnitudes of k_{rot} and k'_{rot} for the higher temperature range, *ca.* −40 to 25 °C, were calculated by extrapolation. These values were then used to simulate theoretical bandshapes and compared with experimental one-dimensional bandshapes (Fig. 2), using the standard

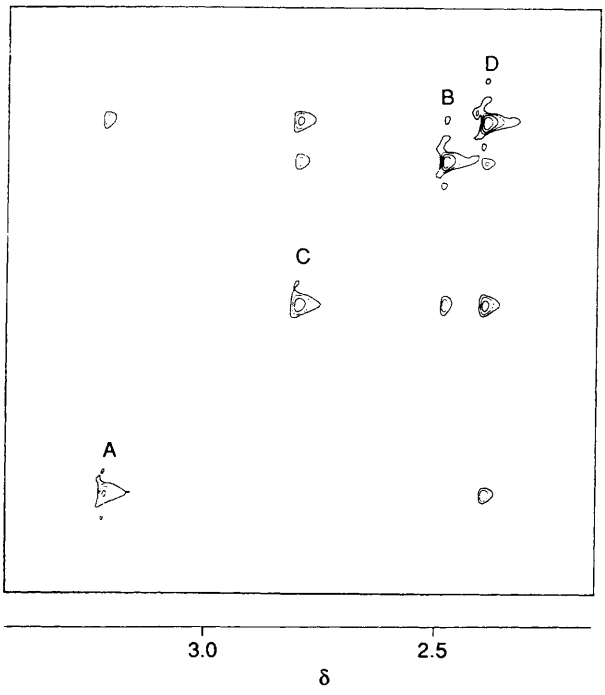

Fig. 4 Two-dimensional EXSY ^{1}H NMR spectrum (SMe region) of $[Pd\{PPh(C_6H_4SMe\text{-}o)_2\}I_2]$ at −85 °C showing the cross-peaks resulting from SMe replacement. The rate of pyramidal S inversion at this temperature is negligibly slow

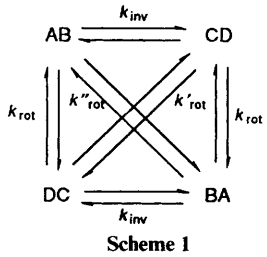

Scheme 1

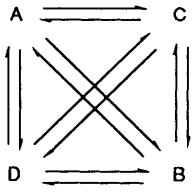

Scheme 2

DNMR3 fitting program.[12] Moderately satisfactory fittings were obtained, but a considerable improvement was achieved by introducing non-zero values of the inversion rate constant, k_{inv}. Sulfur inversion is expected to occur at measurable rates at these higher temperatures so this finding was fully in accord with expectations. By this procedure excellent fittings of the experimental and theoretical spectra were achieved (Fig. 2). The one-dimensional spectra proved to be insufficiently sensitive to values of the rate constant k''_{rot} and as this rate constant was too small to be measured from the two-dimensional EXSY experiments no reliable data could be deduced for this *S*-methyl replacement process of the *trans* isomers. The full set of rate data from both one- and two-dimensional spectra is collected in Table 3.

(*ii*) $[Pt\{PPh(C_6H_4SMe\text{-}o)_2\}Cl_2]$.—Complex **4** was assumed to be isostructural with its palladium(II) analogues. Its NMR properties are similar (Table 2) with both *cis* and *trans*

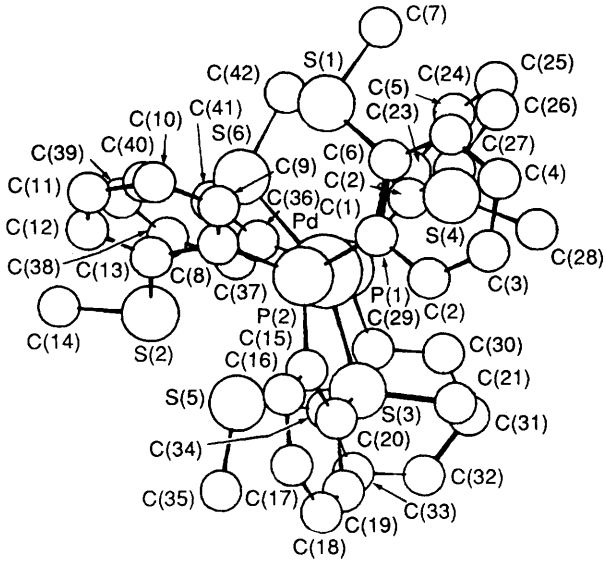

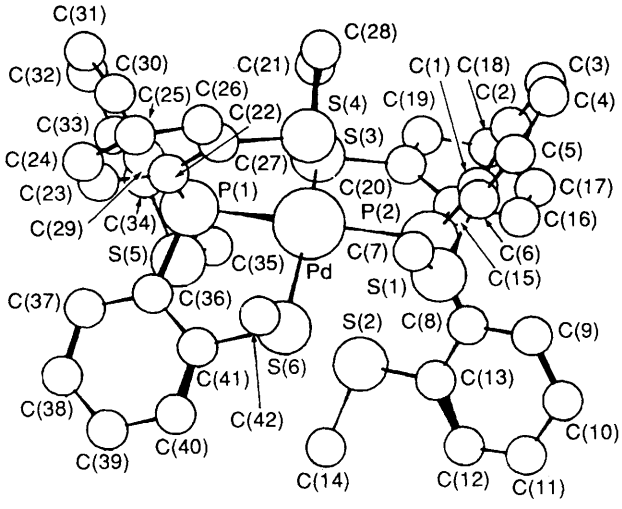

Fig. 5 Two views of the X-ray crystal structure of $[Pd\{P(C_6H_4SMe\text{-}o)_3\}_2][ClO_4]_2$ showing the atom labelling

invertomers present in comparable amounts in solution. Both species show the expected ^3J(Pt–H) coupling of the co-ordinated SMe protons to platinum.

Bandshape fittings of the one-dimensional experimental spectra were attempted but the process was hampered by not having two-dimensional EXSY-based data to work on. However, reasonably good fits of experimental and theoretical spectra in the temperature range 20–65 °C were achieved based on the three SMe replacement rate constants k_{rot}, k'_{rot} and k''_{rot}. Surprisingly, the bandshapes were insensitive to values of k_{inv}.

(*iii*) $[M\{P(C_6H_4SMe\text{-}o)_3\}_2][ClO_4]_2$ (M = Pd *or* Pt).—An X-ray crystal structure determination was carried out on $[Pd\{P(C_6H_4SMe\text{-}o)_3\}_2][ClO_4]_2$ and two views of the structure shown in Fig. 5. Fractional atomic coordinates and selected bond lengths and angles are contained in Tables 4 and 5 respectively. The results show a bis-chelated, square-planar ligand complex with the phosphorus atom and a single sulfur atom from each ligand co-ordinated to the metal. The favoured solid-state structure is the one with the two-co-ordinated thioether moieties *cis* with respect to the planar metallocycle.

Table 3 Rate constants derived from one- and two-dimensional NMR spectra of complexes **1**–**3**

		1			**2**			**3**		
T/°C	τ_m[a]/s	k_{inv}/s^{-1}	k_{rot}/s^{-1}	k'_{rot}/s^{-1}	k_{inv}/s^{-1}	k_{rot}/s^{-1}	k'_{rot}/s^{-1}	k_{inv}/s^{-1}	k_{rot}/s^{-1}	k'_{rot}/s^{-1}
−90	0.16							≈0[b]	1.7[b]	3.2[b]
−85	0.11							≈0[b]	2.6[b]	5.4[b]
−80	0.07							0.8[b]	4.9[b]	8.2[b]
−70						3.5	3.5	6.1	11	23
−60	0.5	≈0[b]	0.3[b]	0.7[b]		10	10	20	70	100
−55						16	16			
−50	0.2	≈0[b]	0.9[b]	2.6[b]		25	25	50	300	300
−45					5.0	40	80			
−40	0.1	0.9[b]	4.0[b]	6.6[b]	10	70	110	300	1250	750
−35					20	110	160			
−30			9.0	19	40	170	280	650	2500	1200
−20			23	40						
−10		10	85	120	520	800	820			
0		30	255	165						
10		250	801	450						

[a] Mixing time for two-dimensional EXSY spectra. [b] Two-dimensional EXSY-based values.

Table 4 Fractional atomic coordinates (× 10^4) for [Pd{P(C$_6$H$_4$SMe-*o*)$_3$}$_2$][ClO$_4$]$_2$

Atom	x	y	z	Atom	x	y	z
Pd	4 341.6(3)	2 191.0(5)	7 578.9(4)	C(27)	3 588(4)	3 309(7)	9 265(6)
P(1)	3 337(1)	2 416(2)	7 553(1)	S(4)	4 345(1)	3 393(2)	9 026(2)
P(2)	5 355(1)	1 953(2)	7 562(2)	C(28)	4 461(9)	4 563(11)	8 980(18)
C(1)	5 767(4)	2 663(6)	8 414(6)	C(29)	2 963(3)	3 119(6)	6 653(6)
C(2)	6 049(4)	3 481(6)	8 151(7)	C(30)	2 729(4)	3 989(6)	6 859(7)
C(3)	6 342(5)	4 078(7)	8 768(7)	C(31)	2 484(5)	4 564(8)	6 186(8)
C(4)	6 365(5)	3 889(8)	9 693(8)	C(32)	2 502(6)	4 283(9)	5 278(9)
C(5)	6 079(5)	3 110(8)	10 000(7)	C(33)	2 722(5)	3 418(8)	5 041(7)
C(6)	5 775(4)	2 492(6)	9 394(6)	C(34)	2 963(4)	2 828(6)	5 731(6)
S(1)	5 429(1)	1 474(2)	9 776(2)	S(5)	3 239(1)	1 710(2)	5 463(2)
C(7)	5 219(5)	1 795(10)	10 894(7)	C(35)	3 530(6)	1 887(10)	4 373(7)
C(8)	5 666(4)	781(6)	7 633(6)	C(36)	3 021(4)	1 253(6)	7 469(6)
C(9)	6 203(5)	622(7)	8 166(7)	C(37)	2 457(4)	1 057(7)	7 104(6)
C(10)	6 453(5)	−263(9)	8 223(8)	C(38)	2 262(7)	137(7)	7 051(7)
C(11)	6 141(7)	−997(9)	7 776(9)	C(39)	2 628(5)	−589(7)	7 384(7)
C(12)	5 622(6)	−856(8)	7 256(8)	C(40)	3 197(5)	−389(7)	7 755(7)
C(13)	5 389(5)	32(7)	7 156(7)	C(41)	3 389(4)	514(6)	7 825(6)
S(2)	4 761(2)	266(2)	6 384(2)	S(6)	4 115(1)	772(2)	8 347(2)
C(14)	4 456(8)	−855(11)	6 043(12)	C(42)	3 917(5)	934(8)	9 536(7)
C(15)	5 558(4)	2 411(6)	6 461(6)	Cl(1)	4 301(1)	3 803(2)	2 760(2)
C(16)	6 112(4)	2 240(8)	6 143(6)	O(1)	3 724(4)	3 464(7)	2 498(6)
C(17)	6 244(5)	2 639(8)	5 339(8)	O(2)	4 657(4)	3 080(6)	3 122(7)
C(18)	5 862(5)	3 205(8)	4 844(8)	O(3)	4 281(4)	4 518(7)	3 415(7)
C(19)	5 305(5)	3 379(7)	5 127(6)	O(4)	4 550(5)	4 155(9)	1 980(7)
C(20)	5 163(4)	2 978(6)	5 949(6)	Cl(2)	3 148(1)	−3 293(2)	7 518(2)
S(3)	4 422(1)	3 118(2)	6 276(2)	O(5)	2 940(6)	−3 145(9)	6 610(9)
C(21)	4 412(7)	4 349(9)	6 532(13)	O(6)	3 592(8)	−2 611(12)	7 661(11)
C(22)	3 166(4)	2 889(6)	8 663(6)	O(7)	3 313(10)	−4 142(15)	7 855(15)
C(23)	2 585(5)	2 783(8)	8 928(7)	O(8)	3 601(11)	−3 948(16)	7 360(16)
C(24)	2 458(5)	3 059(10)	9 794(8)	O(9)	2 892(12)	−3 987(18)	8 144(17)
C(25)	2 892(5)	3 423(9)	10 399(8)	O(10)	3 189(8)	−2 555(12)	8 173(12)
C(26)	3 455(5)	3 555(7)	10 147(7)	O(11)	2 599(16)	−3 171(23)	7 780(22)

Occupancies of disordered oxygens: O(5) 0.88, O(6) 0.57, O(7) 0.43, O(8) 0.39, O(9) 0.40, O(10) 0.54 and O(11) 0.45.

The square plane containing the metal is considerably distorted, the S(3)–Pd–S(6) angle being contracted to only 153.6°, presumably in an attempt to reduce steric crowding. In contrast, the P(2)–Pd–P(1) bond angle is near ideal at 178.4°. The bonds from Pd to S(3) and S(6) are 2.3–2.4 Å. The value of 2.708 Å quoted for the Pd–S(4) distance (Table 5) is interestingly short, and although not depicted as a real bond in Fig. 5 it may represent a close approach towards five-co-ordination of Pd in the solid state. The shortness of this distance will clearly aid the *S*-methyl replacement process (see later). The phosphorus atoms show considerable distortion from ideal tetrahedral geometry, the tetrahedral angle being expanded to 120.9° in the case of C(8)–P(2)–Pd. The phosphorus–palladium bonds lie in the range 2.294–2.321 Å. The lengths of aromatic C–C bonds and C–C–C angles are in their normal ranges. The X-ray data confirmed the existence of two ClO_4^- species as counter ions.

Solution NMR studies. At room temperature the *S*-methyl regions of the ^{1}H NMR spectra of both complexes show a singlet, that of Pt^{II} exhibiting ^3J(Pt–H) coupling. This indicates some averaging process leading to equilibration of the pairs of SMe groups on the two ligands. On cooling both complexes in CD_2Cl_2 solvent the signals broaden and split into three equal-intensity signals (1–3) (Fig. 6). In the case of Pt^{II}, the centre signal shows ^{195}Pt satellites with ^3J(Pt–H) = 43.3 Hz, approximately three times the magnitude of the room-temperature

Table 5 Selected bond distances (Å) and angles (°) for complex **5***

P(1)–Pd	2.294(4)	P(2)–Pd	2.321(4)
S(3)–Pd	2.324(5)	S(4)–Pd	2.708(6)
S(6)–Pd	2.383(4)	C(22)–P(1)	1.816(11)
C(29)–P(1)	1.799(10)	C(36)–P(1)	1.802(11)
C(1)–P(2)	1.796(11)	C(8)–P(2)	1.810(11)
C(15)–P(2)	1.819(12)	S(1)–C(6)	1.759(11)
C(7)–S(1)	1.788(13)	S(2)–C(13)	1.766(12)
C(14)–S(2)	1.791(18)	S(3)–C(20)	1.794(11)
C(21)–S(3)	1.791(15)	S(4)–C(27)	1.782(12)
C(28)–S(4)	1.687(18)	S(5)–C(34)	1.765(11)
C(35)–S(5)	1.781(14)	S(6)–C(41)	1.789(11)
C(42)–S(6)	1.832(13)		
P(2)–Pd–P(1)	178.4(1)	S(4)–Pd–P(1)	82.1(2)
S(3)–Pd–P(2)	85.9(2)	S(4)–Pd–S(3)	106.1(2)
S(4)–Pd–P(2)	99.3(2)	S(6)–Pd–P(2)	97.6(2)
S(6)–Pd–P(1)	82.8(2)	S(6)–Pd–S(4)	99.2(2)
S(6)–Pd–S(3)	153.6(1)	C(29)–P(1)–Pd	119.6(4)
C(22)–P(1)–Pd	108.8(4)	C(36)–P(1)–Pd	105.1(4)
C(1)–P(2)–Pd	111.5(4)	C(8)–P(2)–Pd	120.9(4)
C(20)–S(3)–Pd	106.9(4)	C(15)–P(2)–Pd	106.2(4)
C(28)–S(4)–Pd	125.6(10)	C(21)–S(3)–Pd	112.6(7)
C(42)–S(6)–Pd	114.4(5)	C(27)–S(4)–Pd	99.7(4)
S(3)–Pd–P(1)	93.0(2)	C(41)–S(6)–Pd	101.7(4)

* Estimated standard deviations given in parentheses are applicable to the least significant digits.

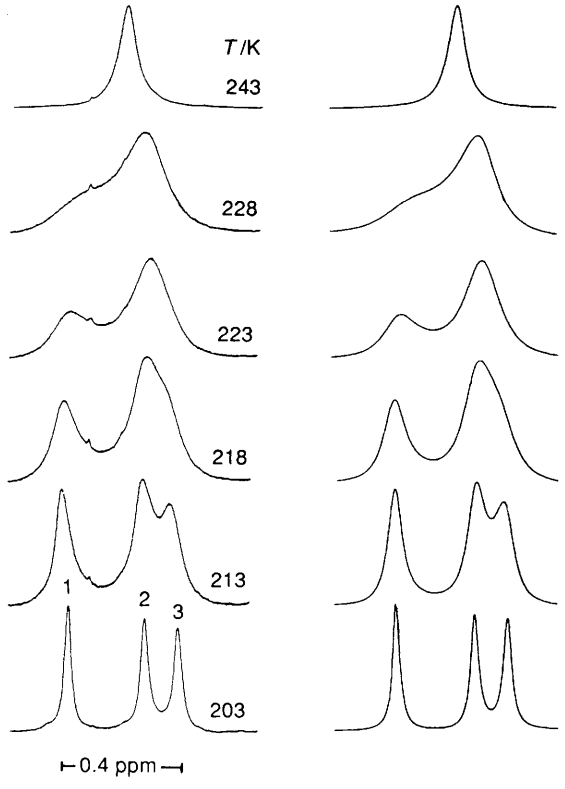

Fig. 6 Experimental and computer-simulated ^{1}H NMR spectra of $[Pd\{P(C_6H_4SMe\text{-}o)_3\}_2][ClO_4]_2$. Lowest-temperature chemical shifts are given in Table 2, best-fit rate constants in Table 6

value. This signal is clearly due to the co-ordinated SMe groups with the other two signals attributed to non-equivalent pairs of unco-ordinated SMe groups (Table 2). At temperatures where pyramidal S inversion is slow, two invertomers, *cis* and *trans* (with respect to the mutual relationship of the co-ordinated SMe groups) may exist. Both species possess two non-equivalent unco-ordinated SMe environments and a single co-ordinated SMe environment, and thus solution NMR spectra

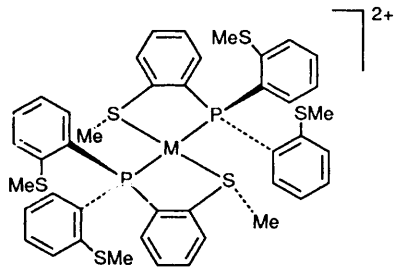

Fig. 7 The *cis* invertomer of $[M\{P(C_6H_4SMe\text{-}o)_3\}_2]^{2+}$ showing the two non-equivalent environments of the pendant SMe groups

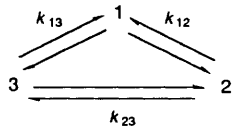

Scheme 3

Table 6 The best-fit rate constants* used in the computer simulation of complexes **5** and **6**

	5			**6**		
T/°C	k_{12}*/s^{-1}	k_{13}*/s^{-1}	k_{23}*/s^{-1}	k_{12}*/s^{-1}	k_{13}*/s^{-1}	k_{23}*/s^{-1}
−60	9.0	17	27			
−55	14	39	65			
−50	30	65	110			
−45	80	110	200			
−40	160	190	390			
−30	620	660	1420	≈0	20	30
−25				40	30	50
−20				70	50	80
−15				130	70	130
−10				230	100	190
−5				330	175	300
5				1000	400	600

* Rate constants refer to Fig. 6 and the dynamic spin problem in the text.

cannot distinguish between them unequivocally. Clearly, the low-temperature solution spectrum is compatible only with the presence of a single species which is assumed to be the *cis* form (Fig. 7) in accord with the solid-state structure. No evidence was found from the ^{1}H NMR spectra for the *trans* invertomer but a ^{31}P-{^{1}H} NMR spectrum of the palladium complex **5** did show a very weak signal at δ 40.8 in addition to the intense *cis* signal at δ 35.0 suggesting very minor abundance (*ca.* 4%) of the *trans* species in CD_2Cl_2 solution.

Dynamic NMR studies. The observed spectral changes with temperature are consistent with the occurrence of an internal methylthio-replacement process analogous to that observed in the $PPh(C_6H_4SMe\text{-}o)_2$ complexes. This process is probably occurring in conjunction with pyramidal inversion of the co-ordinated sulfur atoms but because of the overwhelming abundance of the *cis* invertomer the kinetics of this inversion could not be separately investigated.

First attempts to simulate the dynamic NMR spectra of the two complexes using either one or two independent rate constants for each temperature proved unsatisfactory. Only by using three independent rates for the dynamic spin problem (Scheme 3), where 1 and 3 refer to the chemical shifts of the pendant SMe groups and 2 to the co-ordinated SMe, could satisfactory agreements be achieved between experimental and computer-simulated spectra (Fig. 6). The best-fit rate constants are given in Table 6, where it will be seen that for any temperature they have comparable magnitudes. In view of this the uniqueness of the fittings cannot be guaranteed although considerable efforts were made to test other combinations of rate constant magnitudes.

Table 7 Activation parameters for complexes **1–6**

Complex	Process	E_a/kJ mol^{-1}	$\log_{10}(A/s^{-1})$	$\Delta H^{\ddagger}$/kJ mol^{-1}	$\Delta S^{\ddagger}$/J K^{-1} mol^{-1}	$\Delta G^{\ddagger}$*/kJ mol^{-1}
1	k_{inv}	69 ± 5	15.0 ± 1.0	67 ± 5	36 ± 19	56.6 ± 0.9
	k_{rot}	56 ± 2	13.1 ± 0.4	54 ± 2	−1 ± 7	54.3 ± 0.4
	k'_{rot}	45 ± 1	11.0 ± 0.2	45 ± 1	−41 ± 5	55.6 ± 0.2
2	k_{inv}	67 ± 1	15.9 ± 0.2	65 ± 1	53 ± 3	48.7 ± 0.2
	k_{rot}	41 ± 1	10.9 ± 0.4	39 ± 1	−42 ± 3	51.1 ± 0.2
	k'_{rot}	42 ± 3	11.2 ± 0.6	40 ± 3	−36 ± 12	50.4 ± 0.9
3	k_{inv}	52 ± 3	13.9 ± 0.6	50 ± 3	16 ± 12	45.0 ± 1.0
	k_{rot}	48 ± 3	13.6 ± 0.6	46 ± 3	10 ± 12	42.9 ± 1.1
	k'_{rot}	39 ± 1	11.5 ± 0.4	37 ± 1	−30 ± 7	46.2 ± 0.6
4	k_{rot}	63 ± 3	12.0 ± 0.7	62 ± 2	−23 ± 5	69.3 ± 0.1
	k'_{rot}	57 ± 2	10.9 ± 0.3	54 ± 2	−45 ± 7	67.2 ± 0.1
	k''_{rot}	55 ± 4	10.4 ± 0.5	53 ± 4	−55 ± 11	68.8 ± 0.3
5	k_{12}	63 ± 3	16.4 ± 0.7	61 ± 3	62 ± 13	42.8 ± 1.0
	k_{13}	51 ± 2	13.7 ± 0.4	49 ± 2	11 ± 8	45.5 ± 0.5
	k_{23}	56 ± 2	15.1 ± 0.4	54 ± 2	37 ± 7	42.6 ± 0.5
6	k_{12}	61 ± 2	14.5 ± 0.3	59 ± 2	25 ± 6	51.6 ± 0.2
	k_{13}	48 ± 1	11.7 ± 0.2	46 ± 1	−29 ± 4	54.8 ± 0.2
	k_{23}	48 ± 1	11.8 ± 0.1	46 ± 1	−26 ± 3	53.6 ± 0.1

* Calculated at 298.15 K.

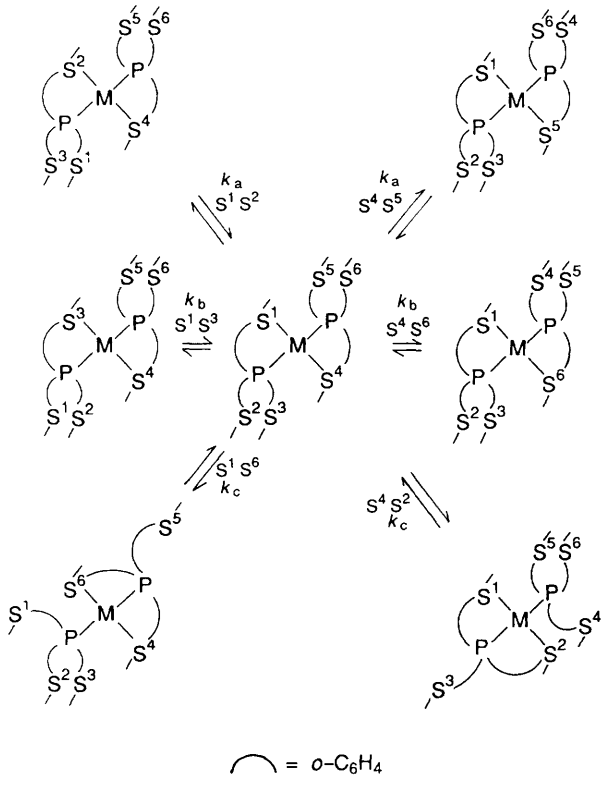

Fig. 8 Mechanistic pathways associated with intra- and inter-ligand SMe replacement processes in $[M\{P(C_6H_4SMe\text{-}o)_3\}_2]^{2+}$ complexes. The labelling S^1S^2, *etc.* refers to the exchange of co-ordinated and unco-ordinated methylthio groups MeS^1 and MeS^2

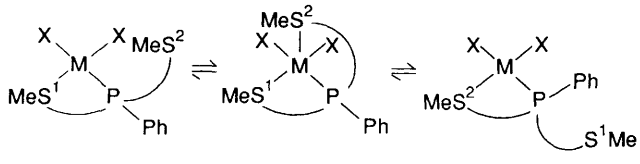

Fig. 9 A possible associative mechanism for SMe replacement in the complexes $[M\{PPh(C_6H_4SMe\text{-}o)_2\}X_2]$

The need for three independent rate constants to characterise each exchange-broadened spectrum suggests a rather complex dynamic scheme in operation. This clearly arises from the many possibilities of pairwise exchange of the six *S*-methyl groups in these complexes. These exchanges depicted in Fig. 8 can involve SMe replacements both within each $P(C_6H_4SMe\text{-}o)_3$ ligand and between both ligands. Starting with the structure at the centre of the scheme with the SMe groups labelled 1–6, intra-ligand replacements can be of two types, characterised by rates k_a and k_b. These rates need not be equal as the processes involve different spatial movements of the pairs of SMe groups after the initial M–S bond easing. The third type of rate constant k_c may be envisaged as arising from an inter-ligand SMe replacement, *viz.* S^1S^6 or S^4S^2 (Fig. 8). In theory, inter-ligand replacements of types S^1S^5 and S^4S^3 are also possible, but these were assumed to be kinetically indistinguishable from the others. The inter-ligand replacement process leads, after initial M–S bond breaking, to two inequivalent ligand moieties, one tri- and one mono-dentate, the latter being bound solely through the P atom. No trace of such species was seen at low temperatures presumably due to their very low solution abundance.

The scheme in Fig. 8 shows only the initial stages of the full dynamic process. Each of the six resultant species of this Figure will change further by numerous other pathways to produce other species many of which are merely tautomers or permutomers of the original structure and will be NMR indistinguishable.

The rate constants, k_{12}, k_{13} and k_{23}, quoted in Table 6 cannot be directly related to k_a, k_b and k_c (Fig. 8) because of the uncertainty in assigning the signals 1,3 of unco-ordinated SMe (Fig. 6). The intramolecular nature of the exchange process was confirmed by addition of free ligand to the complexes at temperatures both at and below the fast-exchange limit. No exchange between free and bound ligand was seen for either complex.

Activation Parameters for the SMe *Replacement Process.*—The full set of activation parameters, based on the Arrhenius and Eyring rate theories, for both the $PPh(C_6H_4SMe\text{-}o)_2$ and $P(C_6H_4SMe\text{-}o)_3$ complexes, is given in Table 7.[17] The magnitudes of $\Delta G^{\ddagger}$, which is least prone to systematic error, are quite similar for all six complexes. However, several points may be noted. First, in both types of complex the energies for S inversion and SMe replacement decrease in order Pt > Pd and in the order Cl > Br > I as observed on previous occasions.[4] The latter trend reflects the relative *trans* influences of halide groups in metal(II) complexes.[16]

Secondly, in the $PPh(C_6H_4SMe\text{-}o)_2$ complexes, the energies of S inversion and SMe replacement are very similar suggesting that both processes are concerted, with the M–S bond

breaking/remaking that accompanies S inversion initiating the replacement process. The latter probably operates *via* an associative mechanism that involves a short-lived 18-electron five-co-ordinate metal transition state (Fig. 9).

Thirdly, the energy barriers to the SMe replacement process in the $P(C_6H_4SMe\text{-}o)_3$ complexes are significantly lower than those for the $PPh(C_6H_4SMe\text{-}o)_2$ species, except when the strong *trans*-influencing I^- ligand is present. This may be due to the relatively higher ground-state energy of the former compared to the latter complexes, which stems from the appreciable steric crowding in these bulky complexes. The mechanism of SMe replacement in these $P(C_6H_4SMe\text{-}o)_3$ complexes is also thought to be associative involving a five-co-ordinate metal transition state analogous to that shown in Fig. 9.

References

1 E. W. Abel, D. Ellis, K. G. Orrell and V. Šik, *Polyhedron*, 1991, **10**, 1603.
2 T. N. Lockyer, *Aust. J. Chem.*, 1974, **27**, 259.
3 G. Dyer, M. O. Workman and D. W. Meek, *Inorg. Chem.*, 1967, **6**, 1404.
4 E. W. Abel, S. K. Bhargava and K. G. Orrell, *Prog. Inorg. Chem.*, 1984, **32**, 1.
5 K. G. Orrell, *Coord. Chem. Rev.*, 1989, **96**, 1.
6 D. W. Meek, G. Dyer and M. O. Workman, *Inorg. Synth.*, 1976, **16**, 165.
7 J. R. Doyle, P. E. Slade and H. B. Jonassen, *Inorg. Synth.*, 1960, **6**, 216.
8 S. E. Livingstone and T. N. Lockyer, *Inorg. Nucl. Chem. Lett.*, 1967, **3**, 35.
9 E. W. Abel, T. P. J. Coston, K. G. Orrell, V. Šik and D. Stephenson, *J. Magn. Reson.*, 1986, **70**, 34.
10 E. W. Abel, I. Moss, K. G. Orrell, V. Šik and D. Stephenson, *J. Chem. Soc., Dalton Trans.*, 1987, 2695.
11 K. G. Orrell, V. Šik and D. Stephenson, *Prog. Nucl. Magn. Reson. Spectrosc.*, 1990, **22**, 141.
12 D. A. Kleier and G. Binsch, DNMR3, Program 165, Quantum Chemistry Program Exchange, Indiana University, 1970.
13 V. Šik, Ph.D. Thesis, University of Exeter, 1979.
14 G. M. Sheldrick, SHELX 84, Program for Crystal Structure Solution, personal communication.
15 G. M. Sheldrick, SHELX 76, Program for Crystal Structure Determination and Refinement, University of Cambridge, 1976.
16 E. W. Abel, S. K. Bhargava, K. Kite, K. G. Orrell, V. Šik and B. L. Williams, *Polyhedron*, 1982, **1**, 289.
17 G. Binsch and H. Kessler, *Angew Chem., Int. Ed. Engl.*, 1980, **19**, 411.

Received 14*th October* 1991; *Paper* 1/05199G